N93-13584

HIGH RESOLUTION IMAGING AT PALOMAR

Shrinivas R. Kulkarni*

Palomar Observatory, 105-24
California Institute of Technology
Pasadena, CA 91125

Abstract

For the last two years we have embarked on a program of understanding the ultimate limits of ground-based optical imaging. We have designed and fabricated a camera specifically for high-resolution imaging. This camera has now been pressed into service at the prime focus of the Hale 5-m telescope. We have concentrated on two techniques: the Non-Redundant Masking (NRM) and Weigelt's Fully Filled Aperture (FFA) method. The former is the optical analog of radio interferometry and the latter is a higher order extension of the Labeyrie autocorrelation method. As in radio Very Long Baseline Interferometry (VLBI), both these techniques essentially measure the closure phase and, hence, true image construction is possible. We have successfully imaged binary stars and asteroids with angular resolution approaching the diffraction limit of the telescope and image quality approaching that of a typical radio VLBI map. In addition, we have carried out analytical and simulation studies to determine the ultimate limits of ground-based optical imaging, the limits of space-based interferometric imaging, and investigated the details of imaging tradeoffs of beam combination in optical interferometers.

Introduction

High-resolution imaging at optical wavelengths is clearly a technique of immense importance for astrophysics. Turbulence in the atmosphere degrades the angular resolution of ground based telescopes, e.g., the angular resolution of the Hale 5 m telescope at 6000 Å is about 33 mas whereas, in practice, the angular resolution is no better than 1 arcsec. This discrepancy between theory and practice has been frustrating for astronomers especially since many questions in astrophysics can only be answered with high angular resolution imaging.

---

*Alfred P. Sloan Fellow and NSF Presidential Young Investigator Fellow

At optical wavelengths, Labeyrie showed that the corruption of the wavefront by the atmosphere can be overcome with his speckle autocorrelation technique. However, the autocorrelation technique cannot produce true images. At radio wavelengths, atmospheric corruption is also severe, especially in VLBI. Despite this, radio astronomers have been able to obtain true images from VLBI data by using "closure phases" - a technique invented by Jennison and vigorously exploited for VLBI applications by the Caltech VLBI group. Closure phase imaging and the closely related technique of self-calibration (see Pearson and Readhead 1984 for a review) now form the basis of all radio imaging.

Given our close association with radio astronomical imaging, we started a group at Caltech two years ago with a view of applying the eminently successful radio imaging techniques to optical wavelengths. The following people constitute the group: A. Ghez, P. Gorham, S. Kulkarni, T. Nakajima, G. Neugebauer, J.B. Oke, T. Prince and A. Readhead. We have concentrated on two different techniques: the Non-Redundant Masking (NRM) and the Fully Filled Aperture (FFA) technique. Each has its own strengths and weaknesses.

The NRM technique is the exact analogue of a linked radio interferometer like the Very Large Array (VLA). The interfering fringes formed by light from a number (5 to 8) of small sections of the Hale 5-m telescope are recorded by a photon-counting detector. Just as in VLBI, closure phases are evaluated every coherence time interval and images are made using VLBI software developed at Caltech.

The FFA technique makes full use of the collecting area of the telescope. This is a higher-order extension of Labeyrie's speckle interferometry technique with the principle advantage that the closure phases can be measured. Thus, true imaging is possible with the FFA. The method was invented by Weigelt and coworkers (e.g., Lohmann, Weigelt, and Wirnitzer 1983) and is now being experimented by almost all active speckle interferometry groups. In this method, the turbulence caused by the atmosphere defines the baselines in some unknown fashion. We compensate for our ignorance of the perturbing atmospheric phase field by calculating the closure phases of *all* possible triplets of baselines. Thus, FFA reduction necessarily involves supercomputers.

The primary goal of our group has been to understand the sensitivity and the limitations of these techniques with a constant view of getting some astrophysical payoffs in the process. To this end, we have designed and built a camera specifically for optical interferometry and used it in two

successful runs on the Hale 5-m telescope. We have now reconstructed high quality images of binary stars and asteroids at angular resolution approaching the diffraction limit of the Hale 5m telescope. We have carried out analytical and numerical simulations to understand the absolute limiting sensitivity of ground based high resolution imaging and to determine optimal methods of combining beams in optical and IR interferometers. We are now at a stage where we can start defining and begin approaching the practical limitations of ground-based high resolution imaging.

The Prime Focus Camera

The Prime Focus Camera essentially consists of a pair of lenses and a microscope objective to expand the image scale (figure 1). The pair of lenses acts as a transfer lens and transfers the image from the focal place of the telescope to another plane. The *f*-ratio of the telescope at the prime focus is about 13 arcsecs/mm, whereas our detector has an active area of 25 mm. An x80 microscope objective enables us to magnify the stellar image to match the detector's size.

The detector is a position-sensing, resistive anode photomultiplier tube (ITT #FM 4146; see Lampton and Paresce 1974). It consists of a red-extended photocathode (MA-2) followed by a stack of five microchannel plates in a V-Z pattern and terminated by a special two-dimensional resistive anode. Ratios of the charges collected at these four corners are processed by an analog processor built by Surface Science Laboratories to yield the x and y coordinate of the photon. For each primary photoelectron the analog processor generates 20 bits of spatial information and 1 strobe pulse. These are passed to a camera controller designed and built by the Palomar electronics group. The controller appends 12 bits of timing information and stores the resulting event in a FIFO buffer memory, the contents of which are DMAed into a μVax and thence recorded on a magnetic tape for further processing. At suitable intervals, a 32-bit absolute time marker is added to the data stream. The net result is that we are able to deduce the arrival time of the photons to 10 μs, which is more than sufficient for speckle applications.

The overall efficiency of our current system at λ6500 Å is one percent and is primarily determined by the net detector efficiency of two percent with the rest being due to telescope and optics.

The apparatus as described above is used to collect FFA data. For NRM we introduce a mask approximately at the focal plane of the first lens (see figure 1). There is a one-to-one mapping between this plane and the primary telescope with a demagnification factor of about 200. Thus, a hole or aperture in the mask of size 0.5 mm corresponds to an aperture of 10 cm at the primary telescope. The effect of introducing the mask is equivalent to blocking out most of the primary mirror except for the 10-cm patches defined by the mask. Stellar light from these patches interferes, and the resulting fringes are recorded by the photon-counting detector.

Three conditions are necessary to obtain closure phases:

1. The aperture size must be smaller than the spatial coherence scale length of the atmosphere, i.e., less than r_0, the Fried parameter.

2. The frame integration time must be less than τ_0, the temporal coherence scale length of the atmosphere. τ_0 is proportional to r_0 and depending on the wind speed is any value between a few ms to a few tens of milliseconds.

3. The light from these apertures must arrive at the detector with the same path length, i.e., the rays need to be focused. Path length compensation needs to be accurate to $(\lambda/\Delta\lambda)\lambda$ where $\Delta\lambda$ is the bandwidth. Thus the telescope optics need not be perfect to fractional wavelength accuracy as long as narrow bandwidths are employed.

The $n_b = n(n-1)/2$ fringes caused by the interference of the n beams lie on top of each other in the detector plane. In the Fourier or spatial frequency domain the fringes are transformed to δ–functions, the amplitude and phase of which contain information about the structure of the source. The mask hole geometry is so chosen that none of the n_b spatial frequencies coincides i.e., the mask is nonredundant. To increase the spatial frequency coverage, the mask is rotated at a variety of position angles. With about a dozen rotations the entire 5-m aperture can be synthesized. The details of data reduction are discussed in the next section.

Image Construction Software

The NRM data reduction parallels the radio VLBI reduction. The data reduction is done on the Convex supercomputer in the astronomy department at Caltech. An optimal coherent

integration interval τ_0 is chosen by empirically evaluating the power spectrum for a range of τ_0. Once τ_0 is chosen, the data are divided into "frames" by collecting photons that arrive within one coherent integration interval. Each frame is Fourier transformed and the resulting n_b spatial frequency phasors are used to obtain the $n_t = n(n\text{-}1)(n\text{-}2)/6$ "triple products" or the "bispectrum" phasors, the phase of which is the closure phase. After many frames have been processed, the resulting bispectrum vectors are fed to the radio VLBI software. Additional details can be found in Nakajima et al. (1989).

The FFA data reduction is necessarily complicated and requires a true supercomputer. We have used Caltech's NCUBE supercomputer, a 512-node concurrent computer. Each node has the computing speed of a Vax 11/780 and a local memory of 512 kbytes. The reduction consists of several steps:

1. Recover amplitudes from the average autocorrelation functions (ACF) of object and calibrator frames.

2. Compute average object and calibrator bispectrum and thence calibrated closure phases.

3. Recover object Fourier phase from the calibrated object phases through a least-squares minimization procedure.

4. Produce a dirty map through direct Fourier inversion.

5. Deconvolve the true image from the dirty image using standard radio astronomy deconvolution techniques like CLEAN.

In practice, there are many biases, some of which arise from the detector, others from the telescope and, finally, some from the discrete nature of photons. These biases have to be understood before any reliable imaging can be done. Our group has made tremendous efforts to understand these biases and only after a lot of hard work are we in the situation where we have a reasonable idea of these biases. We consider our FFA program as one of our major achievements of this year. The details of our algorithm may be found in Gorham et al. (1989a, c).

At the current time, we calculate only the near-axis bispectrum points, about ~10^4 triple products. Despite this simplification, our present algorithm requires ~5×10^6 floating point operations per frame. A typical data set (~2×10^4 frames) can currently be reduced in ~4 CPU hours. Extending the algorithm to include the full bispectrum would increase this to 5 CPU days!

At the current time, we do not do any kind of "flat fielding" since the detector appears to have a uniform response and there are no glaring artifacts.

Results

We had two observing runs in 1988, one in April and the other in July. We observed a wide variety of objects with the FFA and the NRM methods. Data were obtained in the red region (6500 Å) with a bandwidth of 30 Å. In this section, we summarize the success of our group with the NRM and the FFA method. We end it with a summary of the theoretical work done by our group.

Non-Redundant Mask Method

From the April data, we have been able to successfully construct images of two binaries using the NRM technique. The results are now in press (Nakajima et al. 1989).

ß Corona Borealis. This is a spectroscopic binary with visual magnitude ~3.7 mag. Our synthesized image (figure 2) reveals a binary system with Δm=1.6 mag, position angle =75° and a separation of 231 mas. A restoring beam of 50 mas FWHM was used. The largest spurious component is -2 percent of the maximum. Thus the dynamic range defined as the ratio between the maximum and the largest spurious component is 50:1, which is consistent with the SNR of the observed closure phases.

Hercules. This is a double-lined spectroscopic binary with a visual magnitude of 4.2 mag. Our synthesized image (figure 2) shows a binary system of separation of 71 mas, magnitude difference of 2.5, and position angle 31°. The dynamic range is about 30:1, worse than expected from the SNR of the closure phases. We suspect that the decrease in dynamic range from the theoretically expected value is due to systematic errors in the calibrated amplitudes.

Fully Filled Aperture Method

As mentioned in the previous section, the program to reduce the FFA method took a long time to develop. The results we have obtained certainly have paid off our big investment.

Binary Stars. We have imaged a wide variety of binary stars with separation ranging from three to ten times the diffraction limit of the Hale 5-m telescope. The dynamic range in the *dirty* images is about 25:1. Application of devconvolution procedures is expected to further increase the dynamic range. The dynamic range attained in the FFA method appears comparable to that of objects by the NRM method. This suggests that were it not for the count rate limitation, the dynamic range of our FFA images would be even higher. These results are now being written up for submission to the Astronomical Journal (Gorham et al. 1989a).

Asteroids. Perhaps this is the most exciting science that is coming out of our effort. For 2 Pallas we have achieved a resolution of ~100 mas. The dynamic range of the image is about 15:1. We see evidence of the terminator line (figure 3), consistent with the solar phase angle and inclination of the asteroid at the time of the observation. We observed a maximum projected diameter of 510 km and a minimum of 450 km, consistent with the recent estimates of higher ellipticity for Pallas than had been previously thought. The apparent shape of the asteroid supports the identification as a triaxial ellipsoid.

For 14 Irene, we have achieved a resolution of ~50 mas. We find a maximum diameter of 220 km and a minimum of 135 km, giving an axial ratio for this projection of 1.6. We find a significant asymmetry in the brightness of one half of the asteroid image compared to the other with an apparent magnitude difference of ~0.7. Irene is clearly nonspherical. This is not surprising since its size is below the critical size above which asteroids are expected to be approximately spherical. Both these exciting results will soon be submitted to the journal Icarus (Gorham et al. 1989b).

Unfortunately most of the FFA data we obtained last year appears to have suffered from detector saturation. In our detector, owing to the high gain, a single primary photoelectron results in cascade of about 10^7 secondary electrons. These electrons are depleted along the bores of the five microchannel plates and get replenished on a time scale of several tens of milliseconds. During this time, that pixel is effectively dead. We now find that the counting rate has to be kept below 10^4 Hz to avoid this problem. Thus, we believe that the dynamic range of images obtained from the

FFA method can be even significantly higher than reported here. We are proposing to build a new kind of detector (see last section) to overcome this problem.

Analytical and Simulation Studies

We have made great strides in our theoretical understanding of the sensitivity and limitations of optical and IR interferometry. The following listed theory papers have been either published or prepared for publication:

"Signal to Noise Ratio of the Bispectral Analysis of Speckle Interferometry" by Nakajima (1988). An exact expression for the SNR of the bispectrum phasor is derived including the effects due to photon noise. A computer simulation of the atmosphere phase corruption assuming a realistic model (the Kolmagorov spectrum) was used to gain an understanding of the FFA method. Our results showed that the earlier paper by Wirnitzer was in error and the limiting sensitivity of the FFA is probably about the 13-14th mag.

"Self Noise in Radio and IR interferometers" by Kulkarni (1989). Conventional radio imaging theory ignores the crosstalk between fringe phasors. The approximation is not valid for strong sources. In this paper, we derive an exact expression for the variance in a synthesized image. Our analysis indicates that some of the best VLBI and VLA images are not limited by calibration errors but by the self noise of the source itself. Finally, our analysis gives new insights into the closure phase concept. In particular, we argue that the concept of "unique" closure phases is not a very meaningful one and that especially at low SNR levels typical of IR interferometers all closure phases must be considered.

"Noise in Optical Synthesis Images I. Ideal Michelson Interferometer" by Prasad and Kulkarni (1989). We study the distribution of noise in images produced by an ideal optical interferometer, e.g., a space-based optical interferometer. We explicitly consider the crosstalk between the fringe phasors, and estimate the variance in the synthesized image at an arbitrary pixel. Two extreme cases of beam combination geometry are considered: the first, an ${}^nC_2$ interferometer for which each of the n primary beams is subdivided (n-1) ways and pairs of sub-beams are combined on $n(n-1)/2$ detectors and, the second, an ${}^nC_n$ interferometer for which all the n beams interfere on one detector. We show that in both cases the signal-to-noise ratio (SNR) in the synthesized image is proportional to $\sqrt{L}$ where L is the total number of photons intercepted by

the entire array. However, the distribution of the variance depends on the details of beam combination and whether the zero spatial frequency components are included or not. Thus, our principal conclusion is that beam combination geometry should *not* be a major design issue for any future space-based interferometer. However, given all things equal, we recommend an ${}^nC_2$ interferometer for its uniform variance with a negligible loss in sensitivity.

"Noise in Optical Synthesis Images II. Non-Redundant Masking: Sensitivity and Limitations" by Kulkarni and Kakajima (1989). In this paper we derive the distribution of noise in synthesis images produced from the bispectrum data using the NRM method on large optical telescopes. We show that the variances and covariances depend on the fringe power on other baselines. This dependence poses additional restrictions on the design of non-redundant masks if the net variance has to be minimized. At high photon rates, crosstalk is severe and, as a result, the covariance terms collectively dominate over the variance terms. Despite this, the overall SNR performance in the synthesized image is nearly as good as an ideal Michelson interferometer. The covariance terms contribute significantly even at moderate photon rates. The implication of this result on image construction is discussed. At very low photon rates, the triple products become essentially uncorrelated, despite which the SNR in the synthesized image is considerably worse than that of an image synthesized from an ideal Michelson interferometer. In this regime, the beam combination geometry is important and optimal sensitivity is obtained when the number of beams converging onto the detector is 7 - a result which has important repercussions for beam combination in large interferometers like the proposed European Southern Observatory's Very Large Telescope. Finally, we discuss how the standard NRM method can be extended to include the entire collecting area of large telescopes. We find that the "extended" NRM method is superior to the FFA method at high light levels. At very low light levels, extended NRM (ENRM) gives nominally similar performance as FFA. However, we argue that in reality, FFA is more sensitive than ENRM for faint objects.

"Amplitude Recovery Using the CLEAN Algorithm: Applications to Astronomical Speckle Interferometry" by Gorham et al. (1989c). Labeyrie first showed that the power spectrum of an object corrupted by the atmosphere is the product of the atmospheric+telescope transfer function and the object power spectrum. Traditionally, the deconvolution of the object power spectrum from the measured spectrum is done in the spatial frequency domain or the Fourier domain. This method suffers from problems, especially with data obtained from photon counting detectors which cannot tolerate high photon rates. As a result, the atmospheric+telescope transfer function can be

measured to rather low precision. In such cases it is advantageous to carry out the deconvolution in the ACF domain. We have applied the CLEAN deconvolution algorithm to real data and obtained excellent results.

Plans for the Future

We are now at a stage where we can successfully image objects up to 5th magnitude by NRM method and objects up to 9th magnitude by FFA. These sensitivity limits arise from the following factors:

1. Low Detector Efficiency. The current detector efficiency is only 2 percent. Clearly there is much room for improvement here.

2. Narrow Bandwidth. Currently we employ bandwidths of only 30 Å.

3. Detector Saturation. The current detector saturates at rates of about 10^4 Hz, and this affects the FFA method the most. It prevents us from using strong calibrators which, in turn, limits the calibration procedure - crucial for any decent image construction.

In collaboration with Mike Shao at the Jet Propulsion Laboratory, we are proposing to build a PAPA detector (Papaliolios, Nisenson, and Ebstein 1985). This detector, especially when used with a GaAs front end, is expected to have a net detector efficiency of up to 15 percent and, furthermore, will enable us to operate at wavelengths as long as 0.9 μm. These two effects alone should result in an overall sensitivity gain of a factor of 20.

With help of a grant from the Keck foundation, we are now building a computer-controlled dispersion corrector. This corrector will allow us to employ bandwidths as large as 1000 Å -- resulting in another increase of sensitivity by a factor of three.

We are exploring techniques that combine the best of FFA (high sensitivity, high dynamic range) and NRM (high resolution and high dynamic range). Our preliminary computer simulations show that we can employ masks with aperture sizes many times larger than r_o. Larger apertures will necessarily lead to overlap of the fringe phasors in the spatial frequency domain and loss of fringe visibility. Our simulations show that despite this, the increased photon

rate results in an overall increase in the sensitivity. Another such technique for which we have, in fact, obtained data is the annular mask technique. Both these techniques differ from FFA in that we control the mix between the high and low spatial frequency components. In particular, an annular mask offers the highest angular resolution without visibility degradation from the low spatial frequency components as in the standard FFA.

Finally, we are now turning our attention to the infrared. There is plenty of exciting science and lots of bright sources. An IR run has been scheduled for summer this year. So perhaps the next time we meet I hope I can show you some exciting IR high angular resolution pictures.

The bulk of the work performed by our group has been supported by a generous grant from the W.M. Keck Foundation. I thank Jack Burns for supporting my travel to this meeting.

References

1. Gorham, P.W.; Ghez, A.; Kulkarni, S.R.; Nakajima, T.; Neugebauer, G; Oke, J.B.; Prince, T.A.; Readhead, A.C.S. 1989a (in prep).

2. Gorham, P.W.; Ghez, A.; Kulkarni, S.R.; Nakajima, T.; Neugebauer, G.; Oke, J.B.; Prince, T.A.; Readhead, A.C.S. 1989b (in prep).

3. Gorham, P.W.; Ghez, A.; Nakajima, T.; Kulkarni, S.R.; Neugebauer, G; Oke, J.B., Prince, T.A.; Readhead, A.C.S. 1989c (in prep).

4. Lampton, M.; Paresce, F. 1974. Rev. Sci, Instr. 45:1098.

5. Lohmann, A.W.; Weigelt, G.; Wirnitzer, B. 1983. Appl. Opt. 22:4028.

6. Kulkarni, S.R.; 1989. Astron. J. (submitted).

7. Kulkarni, S.R.; Nakajima, T. 1989 (in prep.).

8. Nakajima, T.; Kulkarni, S.R.; Gorham, P.W.; Ghez, A.M.; Neugebauer, G.; Oke, J.B.; Prince, T.A.; Readhead, A.C.S. 1989. Astron. J. (in press).

9. Nakajima, T. 1988. J. Opt. Soc. Am. A 5:1477.

10. Papaliolios, C,; Nisenson, P.; Ebstein, S. 1985. App. Opt. 24:287.

11. Pearson, T. J.; Readhead, A.C.S. 1984. Ann. Rev. Astr. Ap. 22:97.

12. Prasad, S.; Kulkarni, S.R. 1989. Astron. J. (submitted).

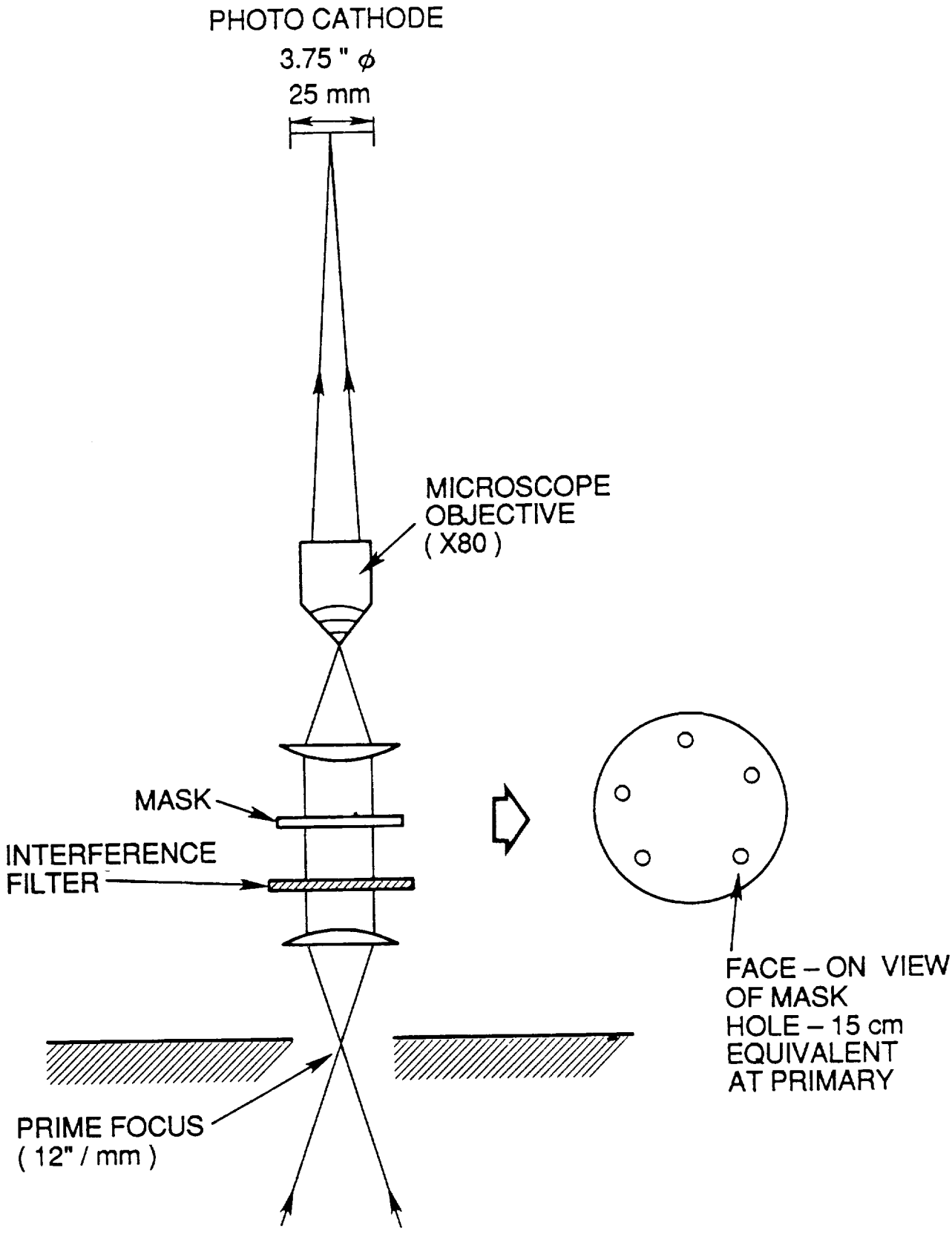

Figure 1: The speckle camera for use at the prime focus of the Hale 5-m telescope.

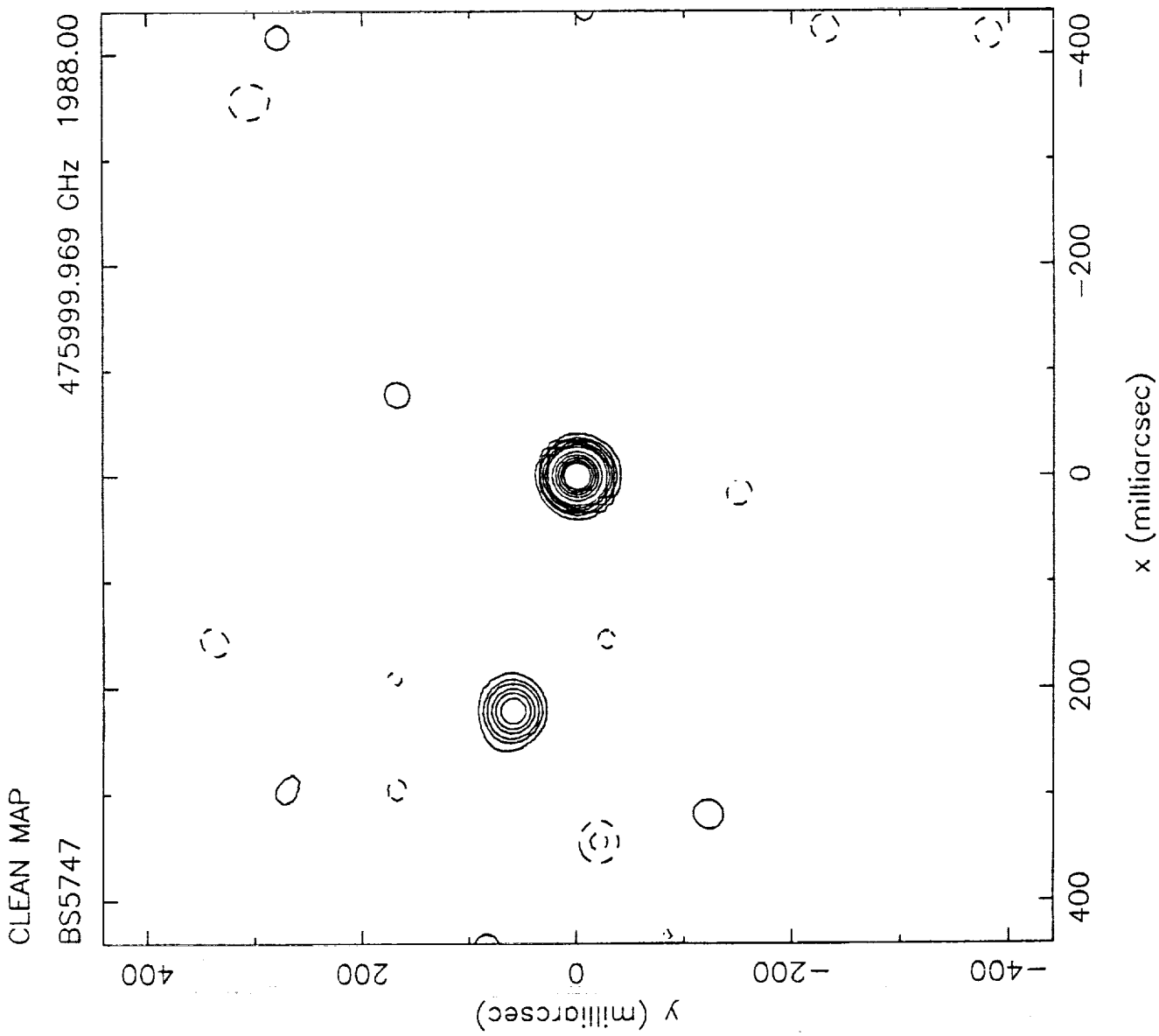

Figure 2a: Image of BS 5747 made using the NRM technique. Dynamic range is about 50:1.

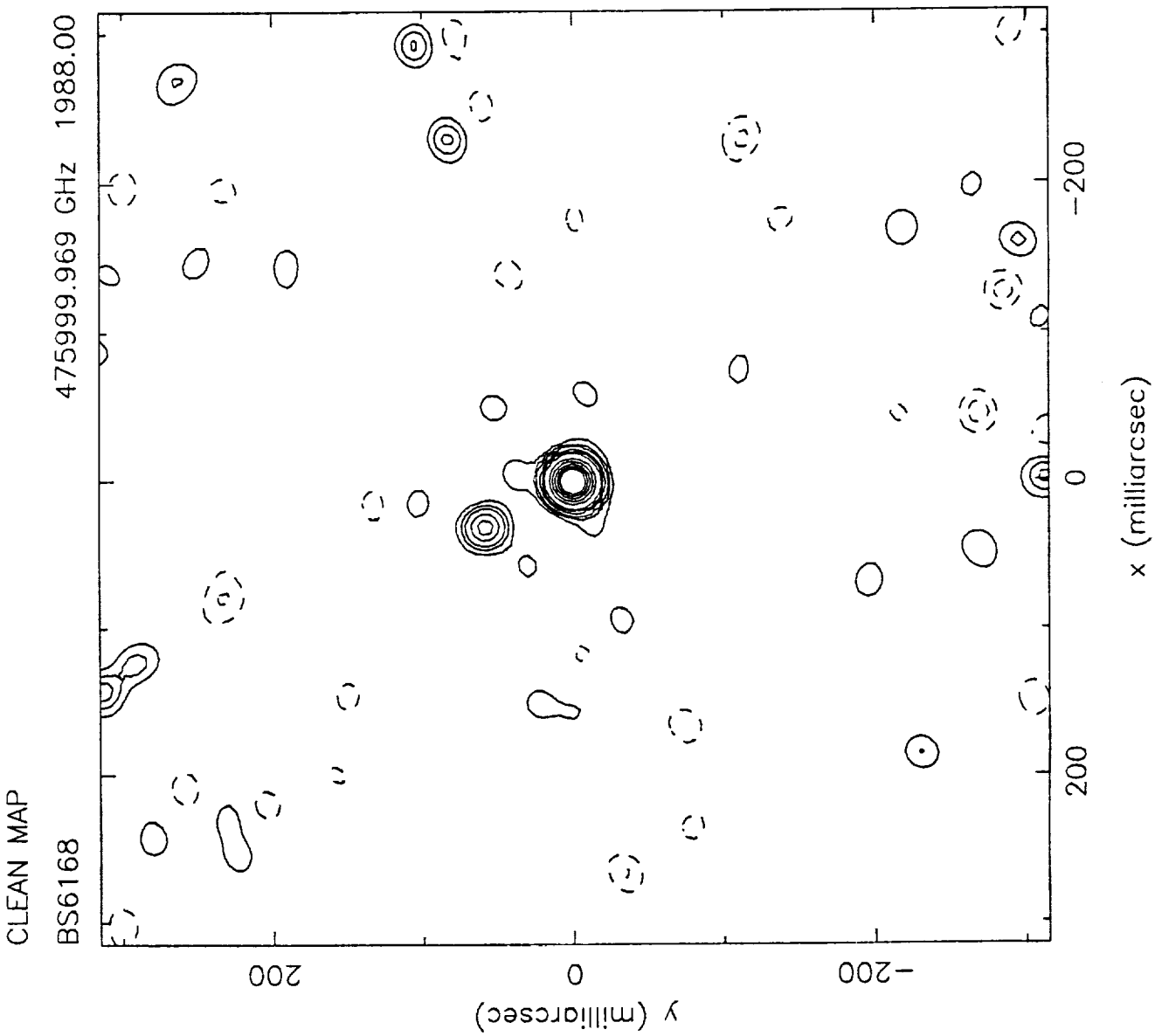

Figure 2b: Image of BS 5747 made using the NRM technique. Dynamic range is about 30:1.

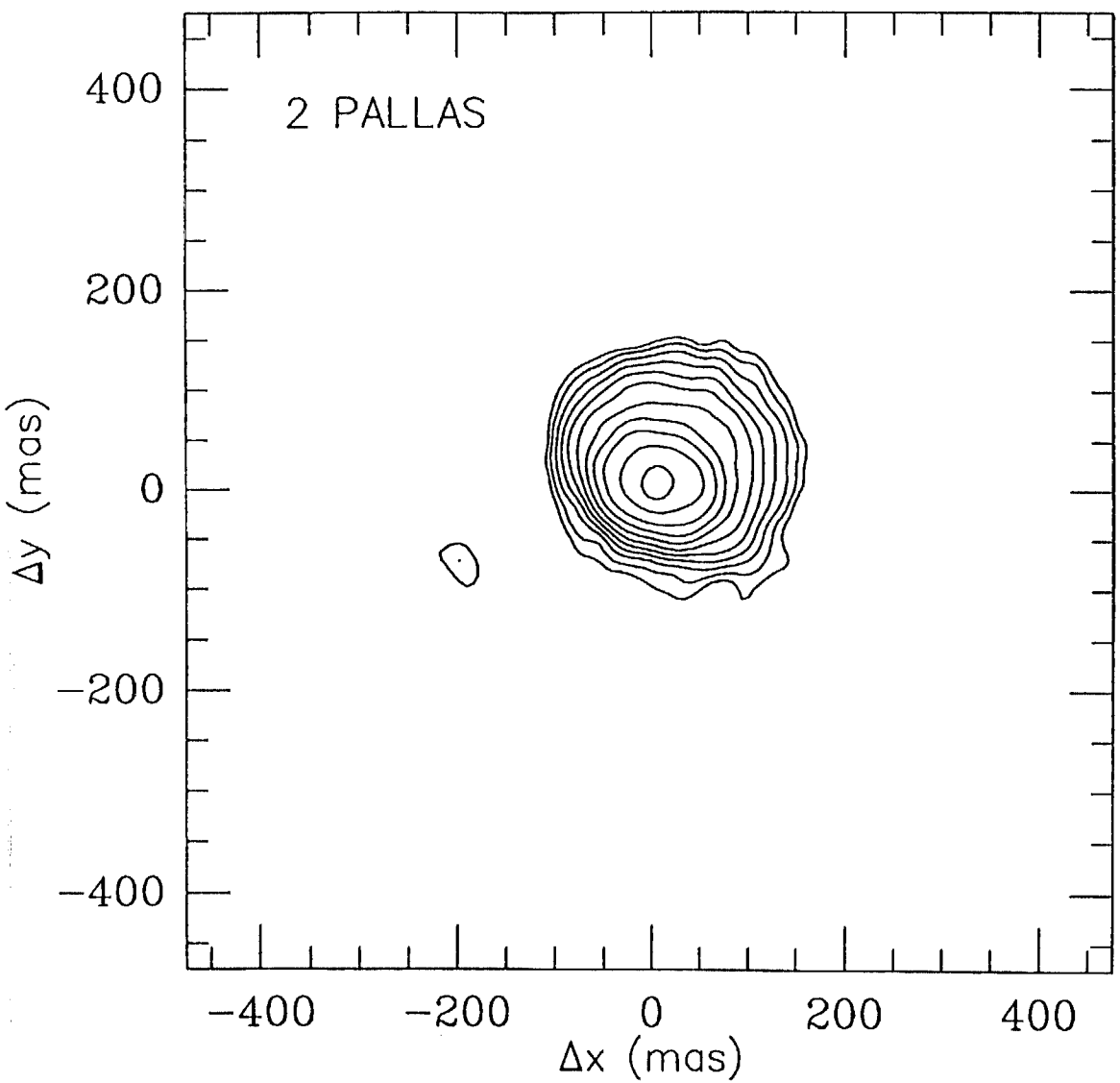

Figure 3: Image of the asteroid 2 Pallas made using the FFA technique. The lowest contour is 10% of the peak. North is up and East to the left. Note that the contours are steeper on the southeastern side as compared to the northwestern side. We explain this asymmetry due to illumination of the asteroid by the Sun.